Screening properties and phase transitions in unconventional plasmas for Ising-type quantum Hall states

Egil V. Herland, Egor Babaev, Parsa Bonderson, Victor Gurarie, Chetan Nayak, and Asle Sudbø

Screening properties and phase transitions in unconventional plasmas for Ising-type quantum Hall states

Egil V. Herland,[1] Egor Babaev,[2, 3] Parsa Bonderson,[4] Victor Gurarie,[5] Chetan Nayak,[4, 6] and Asle Sudbø[1]

[1]*Department of Physics, Norwegian University of Science and Technology, N-7491 Trondheim, Norway*
[2]*Physics Department, University of Massachusetts, Amherst, Massachusetts 01003, USA*
[3]*Department of Theoretical Physics, The Royal Institute of Technology, 10691 Stockholm, Sweden*
[4]*Station Q, Microsoft Research, Santa Barbara, California 93106-6105, USA*
[5]*Department of Physics, CB 390, University of Colorado, Boulder, Colorado 80309, USA*
[6]*Department of Physics, University of California, Santa Barbara, California 93106, USA*

Utilizing large-scale Monte-Carlo simulations, we investigate an unconventional two-component classical plasma in two dimensions which controls the behavior of the norms and overlaps of the quantum-mechanical wavefunctions of Ising-type quantum Hall states. The plasma differs fundamentally from that which is associated with the two-dimensional XY model and Abelian fractional quantum Hall states. We find that this unconventional plasma undergoes a Berezinskii-Kosterlitz-Thouless phase transition from an insulator to a metal. The parameter values corresponding to Ising-type quantum Hall states lie on the metallic side of this transition. This result verifies the required properties of the unconventional plasma used to demonstrate that Ising-type quantum Hall states possess quasiparticles with non-Abelian braiding statistics.

PACS numbers:

I. INTRODUCTION

Key properties of physical systems can sometimes be understood by mapping them to seemingly unrelated ones. A powerful example of this was provided by Laughlin, who observed that the squared norm of his $\nu = 1/M$ fractional quantum Hall trial wavefunction

$$\Psi(z_i) = \prod_{i<j}^{N}(z_i - z_j)^M \, e^{-\frac{1}{4}\sum_{i=1}^{N}|z_i|^2} \tag{1}$$

(where $z_i = x_i + iy_i$ is a complex coordinate in the two-dimensional plane) could be expressed as the Boltzmann weight of a two-dimensional one-component plasma[1]:

$$\|\Psi(z_i)\|^2 = \int \prod_{i=1}^{N} d^2 z_i \, |\Psi(z_i)|^2 = \int \prod_{i=1}^{N} d^2 z_i \, e^{-\beta V_1(z_i)} \tag{2}$$

where

$$V_1(z_i) = -Q_1^2 \sum_{i<j}^{N} \ln|z_i - z_j| + \frac{Q_1^2}{4M} \sum_{i=1}^{N} |z_i|^2 \tag{3}$$

and $Q_1^2/T = 2M$. This mapping allows properties such as quasiparticle charge and braiding statistics to be determined by appealing to the known properties of a one-component plasma.

Recently, a similar plasma mapping was established[2] for Ising-type quantum Hall states, such as the Moore-Read (MR)[3], anti-Pfaffian[4,5], and Bonderson-Slingerland (BS) hierarchy[6] states, which are likely candidates to describe Hall plateaus in the second Landau level, in particular at filling fraction $\nu = 5/2$[7–10]. In this case, the mapping is to a two-dimensional (2D) two-component plasma, where the two species of particles, w and z,

carry not only different values of charge, but also interact through two different interactions, both of the Coulomb form, so the potential energy is:

$$V(z_i; w_a) = V_1(z_i) + V_2(z_i; w_a), \tag{4}$$

$$V_2(z_i; w_a) = -Q_2^2 \sum_{i<j}^{N} \ln|z_i - z_j| - Q_2^2 \sum_{a<b}^{N} \ln|w_a - w_b|$$
$$+ Q_2^2 \sum_{a,i}^{N} \ln|z_i - w_a|, \tag{5}$$

where $Q_2^2/T = 3$. The z-particles interact with each other through the first Coulomb-like interaction, $V_1(z_i)$, given in Eq. (3) (and so does not depend on the w_a coordinates). Moreover, the z-particles interact with each other and with the w-particles through the second Coulomb-like interaction, through which the w-particles also interact with each other, according to $V_2(z_i; w_a)$, given in Eq. (5). Note that $V_2(z_i; w_a)$ is the 2D Coulomb potential of the usual two-component plasma (where the two species carry charge Q_2 and $-Q_2$, respectively).

The z-particles carry charge Q_1 for the first interaction and charge Q_2 for the second interaction. The w-particles carry charge 0 for the first interaction and charge $-Q_2$ for the second interaction. For a plasma with N particles of each species, neutrality is satisfied using a uniform background density of type 1 charge, as in the second term in Eq. (3). This unconventional plasma may be considered as an ordinary neutral two-component gas with positive and negative charges of magnitude Q_2, where the positive charges are given an additional charge of Q_1 that is only felt by the other positive charges and not the negative charges. An illustration of the interactions between the two species in the system is shown in Fig. 1.
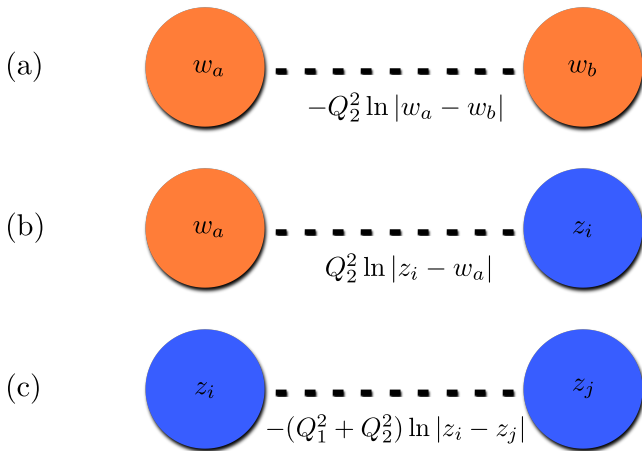
Figure 1: (Color online) Illustration of interactions between the particles in the 2D system. The w-particles only interact by the second Coulomb-like interaction with charge $-Q_2$, whereas the z-particles carry charge Q_1 for the first Coulomb-like interaction and Q_2 for the second Coulomb-like interaction. Thus, the intraspecies interaction among the w-particles, shown in (a), and the interspecies interaction between w and z-particles, shown in (b), are given by Q_2 only, whereas the intraspecies interaction among the z-particles, shown in (c), are determined by Q_1 in addition to Q_2. Interactions between the z-particles and the neutralizing background are omitted from the figure.

We are thus led to consider a class of unconventional plasmas parametrized by Q_1^2/T and Q_2^2/T. As mentioned above, for MR Ising-type states with filling $\nu = 1/M$, the relevant values are $Q_1^2/T = 2M$ and $Q_2^2/T = 3$. In this plasma mapping, the z_i particles in the plasma correspond to the electrons in the MR wavefunctions and the w_a particles correspond to screening operators (fictitious particles). The case $Q_1 = 0$, $Q_2^2/T = 3$ is relevant for the plasma mapping[2] of 2D chiral p-wave superconductors[11]. We note that whenever $Q_1 = 0$, our model is a special case of the well-known 2D two-component plasma of equal and opposite charges[12–15]. The screening properties of multi-component 2D plasmas with multiple Coulomb interactions of this kind are also important for other physical systems, such as rotating multi-component Bose-Einstein condensates with interspecies current-current (Andreev-Bashkin) interaction[16,17] and some multi-component superconducting systems[18–20]. In these systems the screening properties and phase transitions determine superfluid and rotational responses.

In this paper, we fix temperature to $T = 1$ and consider the two most significant values of Q_1, namely $Q_1 = 0, 2$. We investigate the screening and phase transition properties of these plasmas as a function of varying Q_2 by performing a large-scale Monte Carlo simulation. Here, a "screening phase" means that the system has a screening length which is finite, and exponentially decaying effective interactions. A system with logarithmic effective in-

teractions is one where screening is defined to be absent. As a first check, we reproduce the well-known result that, for $Q_1 = 0$, there is a Berezinskii-Kosterlitz-Thouless (BKT) phase transition at $Q_2^2 = Q_{2,c}^2 \approx 4$, as expected for a 2D two-component plasma of equal and opposite charges. For $Q_2^2 < Q_{2,c}^2$, the charges are unbound and the plasma screens, but for $Q_2^2 > Q_{2,c}^2$, the charges are bound into dipoles and the interaction is not screened. Thus, for $Q_2^2 = 3$, the value relevant to 2D chiral p-wave superconductors, the plasma screens. For $Q_1 = 2$, we again find a BKT phase transition at $Q_2^2 = Q_{2,c}^2 \approx 4$, with a plasma screening phase for $Q_2^2 < Q_{2,c}^2$. The first Coulomb-like interaction is deep within its screening phase and appears to have a negligibly small effect on the screening of the second interaction. In both cases, the critical values $Q_{2,c}^2$ are obtained by a finite-size scaling fit of the Monte Carlo data to the BKT form. Our findings demonstrate that the unconventional plasma which occurs in the mapping for both a chiral p-wave superconductor and the Ising-type quantum Hall states is clearly in the screening phase (for both types of Coulomb interaction) and hence allows one to discern the non-Abelian braiding properties of these states, as explained in Ref. 2.

The outline of this paper is as follows. In the introductory part of Section II, we present the model for the unconventional plasma we will be studying in this paper. In Section II A, we connect this to the Ising-type of quantum Hall states. In Section II B, we explain its connection to two-component, two dimensional, Bose-Einstein condensates. In Section III A, we present a formulation of the model on a sphere. In Section III B, we give details of the Monte-Carlo simulations, and in Section III C, we present our results for the screening properties, as well as our findings for the character of phase transition between the dielectric non-screening phase and the metallic screening phase. In Section IV, we present our conclusions. Technical details on the derivation of a generalized dielectric constant is given in Appendix A. In Appendix B, we give a derivation of a relevant higher order response function that we use to characterize the metal-insulator transition. In Appendix C, we present technical details on the finite-size scaling we have used.

II. MODEL

The canonical partition function of the unconventional plasma is written

$$Z = \int \left(\prod_{i=1}^{N} \mathrm{d}^2 z_i \right) \left(\prod_{a=1}^{N} \mathrm{d}^2 w_a \right) \mathrm{e}^{-V}, \qquad (6)$$

where the potential energy V is given by the 2D Coulombic interactions

$$
\begin{aligned}
V = \ & Q_2^2 \sum_{a<b=1}^{N} v_{ww}(|\mathbf{w}_a - \mathbf{w}_b|) \\
& + (Q_1^2 + Q_2^2) \sum_{i<j=1}^{N} v_{zz}(|\mathbf{z}_i - \mathbf{z}_j|) \\
& + Q_2^2 \sum_{a,i=1}^{N} v_{zw}(|\mathbf{z}_i - \mathbf{w}_a|) + V_{z,\mathrm{BG}}.
\end{aligned} \tag{7}
$$

Similar to the study of the 2D two-component neutral Coulomb gas[12–15,21], we introduce a short-range hard-core repulsion between all charges in the system. Treating all charges as hard disks with the same diameter d that limits the range of the hard-core repulsion, the interaction between charges of the same species is

$$
v_{zz}(|\mathbf{r}|) = v_{ww}(|\mathbf{r}|) = \begin{cases} \infty, & |\mathbf{r}| \le d, \\ -\ln|\mathbf{r}|, & |\mathbf{r}| > d, \end{cases} \tag{8}
$$

and the interaction between charges of different species is

$$
v_{zw}(|\mathbf{r}|) = \begin{cases} \infty, & |\mathbf{r}| \le d, \\ \ln|\mathbf{r}|, & |\mathbf{r}| > d. \end{cases} \tag{9}
$$

In Eq. (7), $\mathbf{w}_a$ are position vectors for the particles of component w, and $\mathbf{z}_i$ are position vectors for the particles of component z. To ensure neutrality, the term $V_{z,\mathrm{BG}}$ includes the interaction of the Q_1 charges of type 1 for the z-particles with a neutralizing background charge density. In Ref. 2, this background is a uniform negatively charged 2D disk with charge density $q_1^{\mathrm{BG}} = -NQ_1/A$, where $N/A = 1/2\pi M$, that yields

$$
V_{z,\mathrm{BG}} = \frac{1}{2} \sum_{i=1}^{N} |z_i|^2. \tag{10}
$$

The particle-background and the background-background interaction also yields uninteresting constant terms, that are disregarded in Eq. (7).

We note that when $Q_1 = 0$ we have the 2D two-component neutral Coulomb plasma, which is well-studied both analytically and numerically[12–15,25–30]. At low dipole density, this system will undergo a BKT transition, which is a charge-unbinding transition from a low-temperature state where charges of opposite signs form tightly bound dipoles to a high-temperature state in which a finite fraction of charges are not bound in dipoles, but rather form a metallic state. In the low-temperature phase, this Coulomb gas is an insulator and the dielectric constant ϵ (see for instance Refs. 26,31,32 and Appendix A for a formal definition of ϵ), is finite. In the high-temperature phase, the existence of free charges, yields a conductive gas with an infinite value of ϵ. At the critical temperature T_c, when tightly bound dipoles

starts to unbind, there is a universal jump in the inverse dielectric constant from a non-zero value in the insulating phase to zero in the metallic phase,

$$
\epsilon^{-1} = \begin{cases} 4T_c, & T \to T_c^-, \\ 0, & T \to T_c^+. \end{cases} \tag{11}
$$

The screening properties that follow are that the Coulomb gas is able to perfectly screen test charges in the metallic phase when there are free charges in the system, whereas there is no screening in the insulating dielectric phase. In this work, we will focus our attention on the low dipole density regime, so we will not go into details of the physics in the 2D two-component neutral Coulomb gas at higher densities. However, we note that when density is increased, the critical point of the BKT transition is shifted towards lower temperatures[14,15,28,29].

Another well-studied case is when $Q_2 = 0$, for which the model reduces to the 2D one-component plasma (for the z-particles only). Early numerical studies of this system found a weak first-order melting transition at $Q_1^2/T \approx 140$ from a state where the charges form a triangular lattice with quasi-long-range translational and long-range orientational order to a fluid plasma state[33–36]. These results were, in a sense, contrasting with the defect-mediated melting theory of Kosterlitz-Thouless-Halperin-Nelson-Young (KTHNY) that predicts melting from a solid to a liquid via two BKT-transitions and an intermediate hexatic phase with no translational order and quasi-long-range orientational order[12,37–39]. Other studies of 2D melting point in favor of the KTHNY theory[40–43], suggesting that the nature of melting transition may depend on details in the interatomic potential, or that finite-size effects and lack of equilibration might lead to erroneous conclusions in earlier works. There are also studies that argue for the absence of a phase transition to a low-temperature solid phase in the 2D one-component plasma with repulsive logarithmic interactions because the crystalline state would be unstable to proliferation of screened disclinations for any $T > 0$[44–47].

A. Ising-Type quantum Hall states

The unconventional 2D two-component plasma studied here is mapped to inner products of trial wavefunctions for the MR quantum Hall states using conformal field theory (CFT) methods, as explained in Ref. 2. In particular, this mapping utilizes the Coulomb gas description of CFTs[48,49] together with a procedure for replacing holomorphic-antiholomorphic pairs of contour integrals in screening charge operators for 2D integrals[2,50].

The MR states' wavefunctions can be written as a product of correlation functions of fields from the Ising and U(1) CFTs. In particular, the MR ground-state

wavefunction for N electrons is

$$\Psi(z_1, \ldots, z_N) = \text{Pf}\left(\frac{1}{z_i - z_j}\right) \prod_{i<j}^{N}(z_i - z_j)^M \, e^{-\frac{1}{4}\sum_{i=1}^{N}|z_i|^2} \tag{12}$$

where the Pfaffian of an antisymmetric matrix A is given by

$$\text{Pf}(A_{i,j}) \equiv \frac{1}{N!!} \sum_{\sigma \in S_N} \text{sgn}(\sigma) \prod_{k=1}^{N/2} A_{\sigma(2k-1),\sigma(2k)}. \tag{13}$$

Here, S_N is the symmetric group, σ is one of the permutation elements in S_N, and $\text{sgn}(\sigma)$ is the signature of σ. The $\text{Pf}\left(\frac{1}{z_i - z_j}\right)$ portion of this wavefunction is produced from the correlation function of ψ fields in the Ising CFT, while the Laughlin-type portion

$$\prod_{i<j}^{N}(z_i - z_j)^M \, e^{-\frac{1}{4}\sum_{i=1}^{N}|z_i|^2} \tag{14}$$

is produced from the correlation function of vertex operators in the U(1) CFT.

The Laughlin-type portion of the MR wavefunctions can be mapped to charges of type 1, similar to Laughlin's plasma mapping. The mentioned CFT methods provide identities such as

$$\left|\text{Pf}\left(\frac{1}{z_i - z_j}\right)\right|^2 = \int \prod_{a=1}^{N} d^2 w_a \prod_{a<b}^{N} |w_a - w_b|^3$$
$$\times \prod_{i<j}^{N} |z_i - z_j|^3 \prod_{a,i}^{N} |w_a - z_i|^{-3}, \tag{15}$$

which allow the Pfaffian portion of the MR wavefunctions to be mapped to charges of type 2. This allows one to write the norm of the MR ground-state wavefunction as the partition function of the unconventional 2D two-component plasma of Eq. (4)

$$\|\Psi(z_1, \ldots, z_N)\|^2 = \int \prod_{i=1}^{N} d^2 z_i \, |\Psi(z_1, \ldots, z_N)|^2$$
$$= \int \prod_{a=1}^{N} d^2 w_a \prod_{i=1}^{N} d^2 z_i \, e^{-V}, \tag{16}$$

with $Q_1^2 = 2M$ and $Q_2^2 = 3$. More generally, one can also construct a similar, but more complicated mapping between inner products of wavefunctions of the MR states with quasiparticles, as explained in Ref. 2. In this case, the quasiparticles map to fixed "test" objects in the plasma that carry electric charge of type 1 and can carry both electric and magnetic charges of type 2 (and also changes the number of screening operators, i.e. w-particles in the plasma, to maintain neutrality). (The charges of type 1 and 2 carried by the quasiparticles are typically some fractions of the charges Q_1 and Q_2 carried by the z-particles.)

Strictly speaking, the right-hand-side of Eq. (15) is divergent for $Q_2^2 = 3$ (since the integrand diverges as $|w_a - z_i|^{-3}$ as a w-particle approaches a z-particle). It can be made well-defined (and equal to the left-hand-side) by replacing $|w_a - z_i|^{-3}$ with $|w_a - z_i|^{-\alpha}$, evaluating the integrals for $\alpha < 2$ and then analytically-continuing α to 3. On the other hand, we regularize the divergences of Eq. (16) in this paper by using a hard-core repulsion that forbids the particles from approaching each other closer than a distance d, i.e. replacing V in this expression with that of Eq. (7). It should not matter how we regularize the divergence in Eq. (16) as long as the probability for z-particles and w-particles to sit right on top of each other has measure zero. As we will see in this paper, this is true for $Q_2^2 < Q_{2,c}^2 \approx 4$, in which case the configurational entropy to be gained by having z-particles and w-particles separate overcomes the energy gained by having them on top of each other. We refer to this as an "entropic barrier" for putting z-particles and w-particles on top of each other. In contrast, in Eq. (15), where only the w_is are integrated over and the z_i coordinates are fixed, regularization by a simple hard-core repulsion does not appear to be a suitable alternative to analytic continuation. In this case, since the z_i coordinates are fixed, the entropic barrier is lower. Equivalently, there are fewer integrals to compensate the inverse powers. Thus, in Eq. (15), a simple hard-core cutoff will not reproduce the left-hand-side, and one must use the analytic continuation procedure described above.

B. Two component rotating Bose-Einstein condensate in two dimensions

In a rotating frame, a Bose-Einstein condensate in the London limit is described by the uniformly frustrated XY model,

$$H = \frac{\rho}{2} \int d^2 r \left[\nabla\theta(\mathbf{r}) - \frac{m}{\hbar}\boldsymbol{\Theta}(\mathbf{r})\right]^2, \tag{17}$$

where $\rho = \hbar^2 n/m$ for a condensate with mass m, phase θ and density n, and $\boldsymbol{\Theta}(\mathbf{r}) = \boldsymbol{\Omega} \times \mathbf{r}$ where $\boldsymbol{\Omega} = \Omega\hat{z}$ is the angular velocity of the rotation. In 3D, this model is frequently used to describe the melting of vortex-line lattices in extreme type-II superconductors and superfluids[51–54]. By a duality transformation, the model in Eq. (17) can be rewritten in terms of vortex fields l to yield[55,56]

$$H = \frac{1}{2} \int d^2 q \left[l(\mathbf{q}) - (2\pi)^2 f\delta(\mathbf{q})\right] \frac{\rho}{q^2}$$
$$\times \left[l(-\mathbf{q}) - (2\pi)^2 f\delta(-\mathbf{q})\right], \tag{18}$$

where $f = 2\Omega/\phi_o$ is the vortex number density and $\phi_0 = 2\pi\hbar/m$ is the fundamental quantum unit of vorticity. This is a one-component 2D classical Coulomb

plasma where charges correspond to nonzero values in the vortex field $l(\mathbf{r})$ and the quantity f now plays the role as the neutralizing background charge density.

Extending to two components, a model for a rotating two-component Bose-Einstein condensate with a generic Andreev-Bashkin drag interaction[57–59] reads

$$H = \frac{1}{2} \int \mathrm{d}^2 r \left\{ \sum_{i=1,2} m_i n_i \left(\frac{\hbar \nabla \theta_i}{m_i} - \mathbf{\Theta} \right)^2 - \sqrt{m_1 m_2} n_d \left(\frac{\hbar \nabla \theta_1}{m_1} - \frac{\hbar \nabla \theta_2}{m_2} \right)^2 \right\}, \quad (19)$$

where now m, n and θ is given an index that denotes the component and n_d is the drag density. This model has recently been studied in three dimensions[16,17]. By a duality transformation, we arrive at the following 2D Coulomb plasma

$$H = \frac{1}{2} \int \mathrm{d}^2 q \left[l_i(\mathbf{q}) - (2\pi)^2 f_i \delta(\mathbf{q}) \right] \frac{R_{ij}}{q^2} \times \left[l_j(-\mathbf{q}) - (2\pi)^2 f_j \delta(-\mathbf{q}) \right], \quad (20)$$

where $f_i = 2\Omega/\phi_{0,i}$, $\phi_{0,i} = 2\pi\hbar/m_i$, l_i is the vortex field of component i,

$$R = \hbar^2 \begin{pmatrix} \frac{1}{m_1} \left(n_1 - \sqrt{\frac{m_2}{m_1}} n_d \right) & \frac{1}{\sqrt{m_1 m_2}} n_d \\ \frac{1}{\sqrt{m_1 m_2}} n_d & \frac{1}{m_2} \left(n_2 - \sqrt{\frac{m_1}{m_2}} n_d \right) \end{pmatrix}, \quad (21)$$

and an implicit sum over repeated component indices i, j is assumed. By setting $\hbar = m_i = 1$ such that $f_1 = f_2 = f$, and absorbing a factor $2\pi\beta$ in the density coefficients, we see that the two-component Bose-Einstein condensate in Eq. (19) with $n_1 = 0$, $n_2 = Q_1^2$ and $n_d = -Q_2^2$ corresponds to the unconventional two-component Coulomb plasma in Eq. (7). Thus, the unconventional Coulomb plasma has a counterpart in a two-component Bose-Einstein condensate with a negative non-dissipative drag interaction. However, note that in order to preserve a fixed number of charges when going from the plasma description in Eq. (7) to the phase description in Eq. (19), we have to fix the number of vortices to only include rotationally induced vortices. In principle, in the BEC problem, the system can thermally excite vortex-antivortex pairs, but that process can be substantially suppressed by going beyond the phase only model in Eq. (19) and introducing an additional energy penalty associated with vortex cores.

III. MONTE-CARLO SIMULATIONS

A. Considerations for a spherical surface

Computer simulations of Coulomb interactions are generally difficult to perform due to the long-ranged na-

ture of the interaction. Several techniques have been presented to deal with the complications that arise[60–62]. We have performed large-scale Monte-Carlo simulations of the system described in Eqs. (6) and (7) on a spherical surface. For other simulations on a spherical surface, see Refs. 14,34,43–46,63. This may seem like a brute-force approach since the workload of the simulations scales as $\mathcal{O}(N^2)$. However, the benefit is that there are no boundaries, the implementation is relatively easy, and there is no need to constrain the particles to move on a lattice. However, one must also be aware that simulation results may differ due to effects induced by topology. For instance, the triangular crystalline ground state of a 2D one-component plasma will necessarily include a number of dislocations and disclinations on a sphere. These defects are not present in the ground state when the one-component plasma is located on the plane[45,64].

We consider a sphere with radius R, with origin defined as the center of the sphere such that all particle position vectors $\mathbf{w}_a$ and $\mathbf{z}_i$ are radial vectors with fixed magnitude R in three dimensions. The distance between the particles is measured along the chord[14,63]

$$|\mathbf{r}_i - \mathbf{r}_j| = 2R \sin\left(\frac{\psi_{ij}}{2} \right), \quad (22)$$

where

$$\psi_{ij} = \arccos(\hat{\mathbf{r}}_i \cdot \hat{\mathbf{r}}_j) \quad (23)$$

is the chord angle between the two particles at $\mathbf{r}_i$ and $\mathbf{r}_j$ with unit vectors $\hat{\mathbf{r}}_i$ and $\hat{\mathbf{r}}_j$, respectively. We may now rewrite the model in Eq. (7) on the surface of a unit sphere as

$$V = \frac{1}{2} \left[Q_2^2 \sum_{a<b=1}^{N} \tilde{v}_{ww}(\hat{\mathbf{w}}_a \cdot \hat{\mathbf{w}}_b) + Q_2^2 \sum_{a,i=1}^{N} \tilde{v}_{zw}(\hat{\mathbf{z}}_i \cdot \hat{\mathbf{w}}_a) + (Q_1^2 + Q_2^2) \sum_{i<j=1}^{N} \tilde{v}_{zz}(\hat{\mathbf{z}}_i \cdot \hat{\mathbf{z}}_j) \right], \quad (24)$$

with interactions given by

$$\tilde{v}_{zz}(\hat{\mathbf{r}}_i \cdot \hat{\mathbf{r}}_j) = \tilde{v}_{ww}(\hat{\mathbf{r}}_i \cdot \hat{\mathbf{r}}_j) = \begin{cases} \infty, & \psi_{ij} \leq d/R, \\ -\ln(1 - \hat{\mathbf{r}}_i \cdot \hat{\mathbf{r}}_j), & \psi_{ij} > d/R, \end{cases} \quad (25)$$

and

$$\tilde{v}_{zw}(\hat{\mathbf{r}}_i \cdot \hat{\mathbf{r}}_j) = \begin{cases} \infty, & \psi_{ij} \leq d/R, \\ \ln(1 - \hat{\mathbf{r}}_i \cdot \hat{\mathbf{r}}_j), & \psi_{ij} > d/R. \end{cases} \quad (26)$$

Note that the interaction $V_{z,\mathrm{BG}}$ in Eq. (7) between the neutralizing background and the excess charge of type 1 becomes a constant term on the sphere, so we disregard it in Eq. (24).

The dimensionless density of particles on the sphere is given by the packing fraction $\eta = Ns/A$ where $s = A\sin^2(d/4R)$ is the area of a hard disk of diameter d on

the sphere of area $A = 4\pi R^2$. In the simulation, we use a unit sphere with $R = 1$.

As explained in Appendix A, in order to account for screening properties when particles interact by two interactions simultaneously, we measure a general inverse dielectric constant, $\epsilon^{-1}_{(a_1,a_2)}$, given by

$$\epsilon^{-1}_{(a_1,a_2)} = a_1^2 \epsilon^{-1}_{11} + 2a_1 a_2 \epsilon^{-1}_{12} + a_2^2 \epsilon^{-1}_{22}, \qquad (27)$$

where

$$\epsilon^{-1}_{\mu\nu} = \delta_{\mu\nu} - \frac{\pi}{A} \langle \mathbf{M}_\mu \cdot \mathbf{M}_\nu \rangle, \qquad (28)$$

is a type specific inverse dielectric constant, a_1 and a_2 are type dependent factors that account for the strength one should weigh the $\epsilon^{-1}_{\mu\nu}$ with (given by the charge strength the test particles to measure screening for, may carry in both interactions simultaneously), and where $\mathbf{M}_1$ and $\mathbf{M}_2$ are the dipole moments for charges of type 1 and type 2, respectively, given by

$$\mathbf{M}_1 = Q_1 R \sum_{i=1}^{N} \hat{\mathbf{z}}_i, \qquad (29)$$

$$\mathbf{M}_2 = Q_2 R \left(\sum_{i=1}^{N} \hat{\mathbf{z}}_i - \sum_{a=1}^{N} \hat{\mathbf{w}}_a \right). \qquad (30)$$

Note that the type 2 inverse dielectric constant, ϵ^{-1}_{22}, is the same dielectric constant as was used when studying the two-component neutral Coulomb plasma on a spherical surface[14,63]. In addition to measuring the screening properties, the inverse dielectric constant may be used to identify the existence of a BKT-transition if it exhibits a universal discontinuous jump at the critical point, according to Eq. (11).

In addition to the inverse dielectric constant, we also measure the fourth-order modulus, γ[65,66]. This quantity may be used to verify a discontinuous jump in the inverse dielectric constant without making any *a priori* assumptions regarding the character of the phase transition. As explained in detail in Appendix B, a negative γ at the phase transition in the thermodynamic limit implies that the inverse dielectric constant jumps to zero discontinuously. As for the inverse dielectric constant, we use a general fourth-order modulus to account for the two interactions,

$$\gamma_{(a_1,a_2)} = \sum_{\mu,\nu,\rho,\sigma=1}^{2} a_\mu a_\nu a_\rho a_\sigma \gamma_{\mu\nu\rho\sigma}, \qquad (31)$$

where

$$\gamma_{\mu\nu\rho\sigma} = \left(\frac{\pi}{R^2} \right)^2 [\langle \mathbf{M}_\mu \mathbf{M}_\nu \rangle \langle \mathbf{M}_\rho \mathbf{M}_\sigma \rangle - 3 \langle M_{\mu,z} M_{\nu,z} M_{\rho,z} M_{\sigma,z} \rangle]. \qquad (32)$$

The explicit derivation of Eqs. (31) and (32), is given in Appendix B.

B.   Details of the Monte-Carlo simulations

The Monte-Carlo updating scheme consists of trial moves for one or two particles at the same time, to a randomly chosen new location on the surface of the sphere. The change in the action Eq. (24) was calculated and the move was accepted or rejected according to the Metropolis-Hastings algorithm[67,68]. The trial moves were performed in three different ways. The first way was to move a single particle to a new random location uniformly over the total surface. The second way was to move a single particle to a new random location uniformly within some short distance, adjusted to yield a high acceptance rate. The last trial move was to move a nearest-neighbor pair of one z-particle and one w-particle together, to a random new location uniformly within some short distance, adjusted to yield a high acceptance rate, and with a random new orientation. In order to straightforwardly ensure detailed balance, we additionally required the two particles to mutually be nearest-neighbors both in the old and the new configuration. And to ensure ergodicity, the pair-move must be mixed with a number of single-particle moves. All of these moves were found to be essential in order to have fast thermalization as well as short autocorrelation times for the cases considered here. Pseudorandom numbers were generated by the Mersenne-Twister algorithm[69] and the sampled data were postprocessed using Ferrenberg-Swendsen reweighting techniques[70,71].

C.   Results

Motivated by its relevance to the fractional quantum Hall effect (in particular, the $\nu = 1/2$ MR state), we focus on analyzing the screening properties of this system at $Q_1 = 2$ $(M = 2)^2$. We also perform simulations in the neutral two-component Coulomb gas case at $Q_1 = 0$ $(M = 0)$ in order to provide a check on the numerics, as well as for comparison with the $Q_1 = 2$ case. Furthermore, the system is also studied for a number of values of the packing fraction, η to extract the screening properties in the low-density limit.

For the two cases of Q_1 and the values of Q_2 studied below, the quantities ϵ^{-1}_{11} and ϵ^{-1}_{12} were found to be zero, within statistical uncertainty, and except for a small finite-size effect when system size N, was small. Thus, we focus on the results for ϵ^{-1}_{22} as this was the only term in Eq. (27) that contributed to the general inverse dielectric constant, $\epsilon^{-1}_{(a_1,a_2)}$. This means that screening properties of particles that interact with charges of both types, are determined by the charges of type 2, only. Note also that when $\epsilon^{-1}_{11} = 0$, the unconventional Coulomb plasma will screen test particles with charge of type 1, only.

In Fig. 2, we plot ϵ^{-1}_{22} in the relevant range of Q_2^2 when the two-component neutral Coulomb gas $(Q_1 = 0)$ is known to have a BKT transition. At small values of Q_2^2, the system is in the screening phase where $\epsilon^{-1}_{22} \approx 0$. The
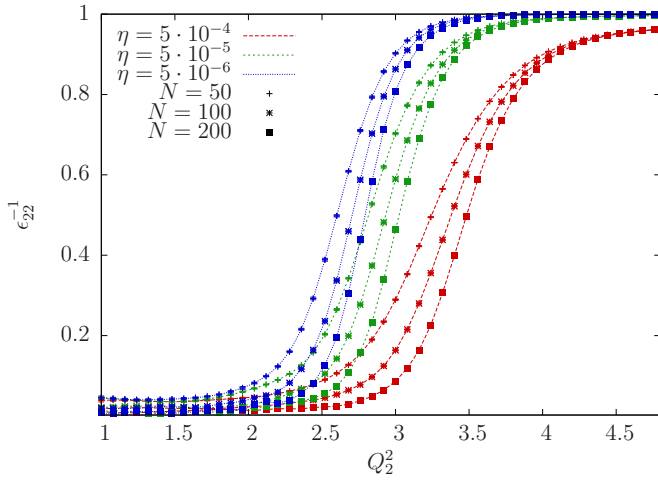
Figure 2: (Color online) Plot of the inverse dielectric constant ϵ_{22}^{-1} for the model in Eq. (7) with $Q_1 = 0$ and $1 \leq Q_2^2 \leq$ 4.8. Results are presented for three different values of packing fraction η and three different values of system size N.

Figure 3: (Color online) Plot of the inverse dielectric constant ϵ_{22}^{-1} for the model in Eq. (7) with $Q_1 = 2$ and $1 \leq Q_2^2 \leq$ 4.8. Results are presented for three different values of packing fraction η and three different values of system size N.

reason for the $\approx$ sign rather than an equal sign is that there is a mainly size-dependent offset from $\epsilon_{22}^{-1} = 0$, because perfect screening is not possible with a small number of charges. For large Q_2^2 there is a phase in which charges of different components form tightly bound dipoles and the Coulomb gas turns into an insulator where $\epsilon_{22}^{-1} \approx 1$. Here, there is a mainly density-dependent offset from $\epsilon_{22}^{-1} = 1$ because the polarizability of the system increases with density, since the hard-core diameter d yields a minimum distance between the charges in the dipoles. The plot in Fig. 2 indeed shows that the charge-unbinding transition is dependent on the number of particles in the system, as well as the size of the hard disk charges. When N increases, the onset of a finite value in ϵ_{22}^{-1} moves to higher values of Q_2^2. However, when we reduce η, the value of Q_2^2 at onset of ϵ_{22}^{-1} becomes smaller. Thus, this figure illustrates that understanding the behavior in both limits $N \to \infty$ as well as $\eta \to 0$ is not straightforward.

In Fig. 3, results for the same case as in Fig. 2 are presented, but with $Q_1 = 2$. The results for $Q_1 = 0$ and $Q_1 = 2$ are very similar, both qualitatively and quantitatively. Thus, the screening properties with respect to charge of type 2 of the unconventional Coulomb plasma when $Q_1 = 2$ are very similar to the well-studied two-component neutral Coulomb gas.

To get a qualitative picture of the type 2 charge binding of the unconventional plasma, three snapshots of the charge configuration when $Q_1 = 2$, $\eta = 5 \cdot 10^{-4}$, and $N = 200$ is given in Fig. 4. When $Q_2^2 = 1$, deep into the screening phase of the system (see Fig. 3), most charges are free and only a small fraction of the charges may be said to form closely bound dipoles. At $Q_2^2 = 3$, which is the relevant value for the Ising-type quantum Hall states, the system is closer to the unbinding transition and a larger fraction (though not all) of the particles are
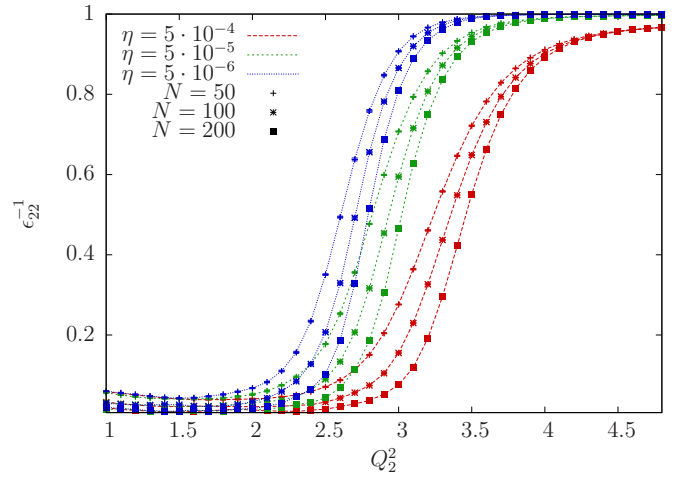
bound in dipoles. At $Q_2^2 = 5$, deep in the type 2 insulating region, all particles form closely bound dipoles and the ability to screen type 2 test charges is lost.

Although it is clear from Figs. 2,3 that there is a transition between a screening phase and an insulating phase, it is not easy to spot the transition point in the curves in these figures, which look rather smooth. Therefore, we must make some assumptions about the nature of the transition in order to identify it.

For the case $Q_1 = 0$, where the transition is known to be a BKT transition, it is natural to follow a method that was proposed in Ref. 72. At the BKT critical point, ϵ_{22}^{-1} scales logarithmically with N for large N. It taked the following finite-size scaling form:

$$\epsilon_{22}^{-1}(N) = \epsilon_{22}^{-1}(\infty)\left[1 + \frac{1}{\ln(N) + C}\right], \qquad (33)$$

where $\epsilon_{22}^{-1}(\infty)$ is the value of $\epsilon_{22}^{-1}(N)$ when $N \to \infty$ and C is an undetermined constant. Least-squares curve-fitting to Eq. (33) may be performed for various sizes N with C and $\epsilon_{22}^{-1}(\infty)$ as free parameters at fixed values of Q_2^2. The critical point is then estimated as the value of Q_2^2 which exhibits the best fit to Eq. (33). Additionally, for a BKT-transition, the value of $\epsilon_{22}^{-1}(\infty)$ obtained at the best fit, must correspond with the universal jump condition, $Q_{2,c}^2\epsilon_{22}^{-1}(\infty) = 4$, cf. Eq. (11). Details of this procedure are given in Appendix C.

For $Q_1 = 2$, motivated by the similarity between Figs. 2, 3, we assume that the transition is also a BKT transition. We again look for the Q_2^2 value at which the system best fits Eq. (33). Since we are able to find a value at which there is a very good fit to this form, we conclude that our assumption was justified.

In Fig. 5, we present results for the critical coupling $Q_{2,c}^2$ for four different densities $\eta = 0.0002, 0.0005, 0.001, 0.002$, for $Q_1 = 0$ and $Q_1 = 2$. The
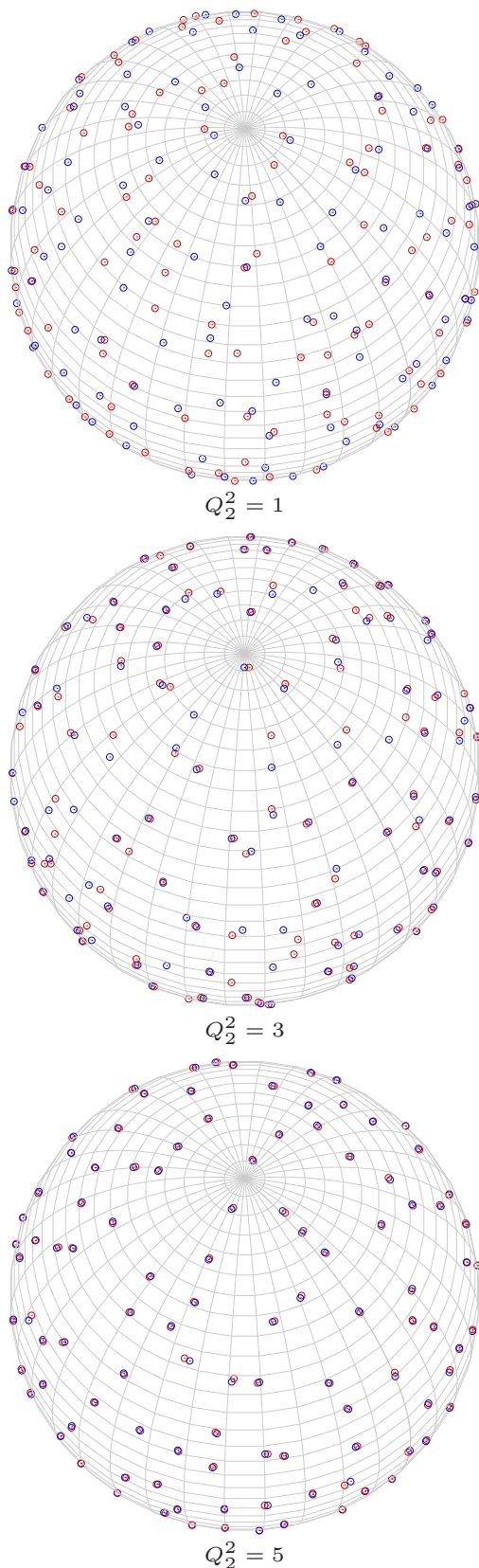
$Q_2^2 = 1$

$Q_2^2 = 3$

$Q_2^2 = 5$

Figure 4: (Color online) Snapshots of the charge configuration at $Q_2^2 = 1, 3, 5$ when $Q_1 = 2$, $\eta = 5 \cdot 10^{-4}$ and $N = 200$. Red markers represent w-particles, while blue markers represent z-particles. The marker diameters are about 5 times larger than hard disk diameter d.
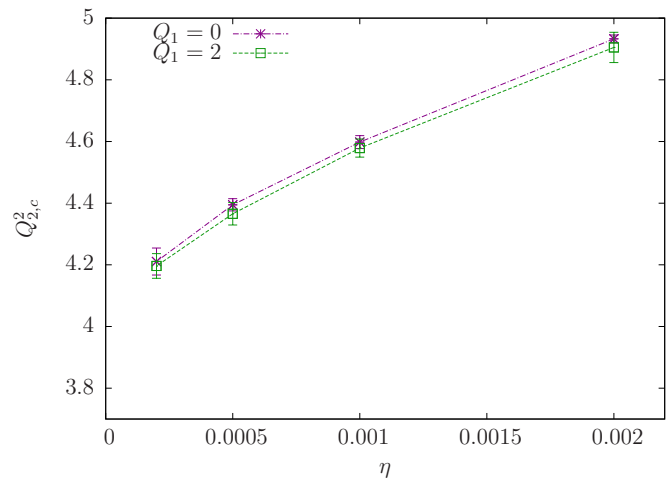

Figure 5: (Color online) The critical value of Q_2^2 found by curve fitting to Eq. (33) with two free parameters. Results are presented for four values of the packing fraction η and for $Q_1 = 0$ and $Q_1 = 2$. Fourteen system sizes in the range $20 \leq N \leq 2000$ have been used.

results for $Q_1 = 0$ reproduce the main features of the two-component Coulomb gas, namely that $Q_{2,c}^2 = 4$ when density is low and that $Q_{2,c}^2$ increases when density increases. These results also correspond well with earlier results in Refs. 14 and 15. When $Q_1 = 2$, we find that the behavior of the critical temperature is very similar to the $Q_1 = 0$ case, within statistical uncertainty. In addition, in Fig. 6, results for the corresponding value of the parameter $\epsilon_{22}^{-1}(\infty)$ at the critical point is presented. The values for both $Q_1 = 0$ and $Q_1 = 2$ are close to the universal value of $Q_{2,c}^2 \epsilon_{22}^{-1}(\infty) = 4$ for the BKT-transition. Since the results for $Q_1 = 0$ (the standard Coulomb-plasma BKT-transition case) and $Q_1 = 2$ are essentially the same, we suggest that the charge-unbinding transition for the unconventional Coulomb plasma indeed is a BKT-transition in the sense that the type 2 inverse dielectric constant ϵ_{22}^{-1} exhibits logarithmic finite-size scaling and a discontinuous jump with a universal value, as predicted by the BKT renormalization equations.

As an additional verification of the discontinuous jump in the BKT-transition, we also study the fourth-order modulus $\gamma_{(a_1,a_2)}$, presented in Eqs. (31) and (32). As for the general inverse dielectric constant, we found that the only contributing term in the sum of Eq. (31) is the term with all indices equal to 2, γ_{2222}. Illustrating the typical behavior of this quantity, results for γ_{2222} for a number of sizes when $\eta = 5 \cdot 10^{-4}$ and $Q_1 = 2$ are presented in Fig. 7. Typically, γ_{2222} exhibits a dip at a value of the coupling that can be associated with the transition. As explained in Appendix B, a negative and finite dip in the limit when $N \to \infty$ signals the discontinuous jump in ϵ_{22}^{-1} that is a characteristic feature of a BKT-transition. To this end, the size of the dip in γ_{2222} is plotted as a function of inverse system size N^{-1} in Fig. 8 in the case when $\eta = 5 \cdot 10^{-4}$. The size of the dip $|\gamma_{2222,\min}|$ decreases when
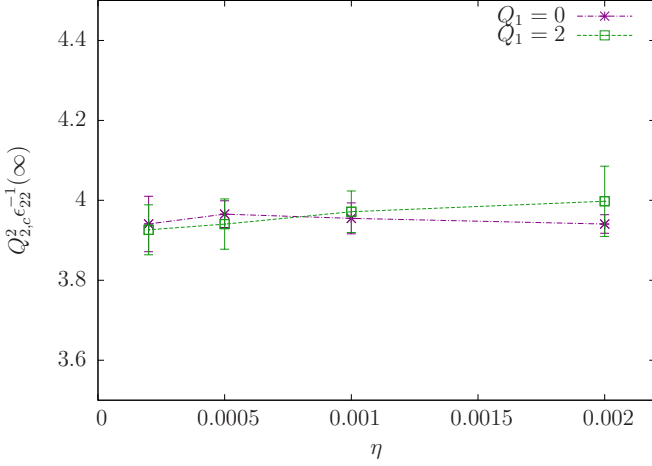
Figure 6: (Color online) The universal jump value determined by curve fitting to Eq. (33) with two free parameters. Results are presented for four values of the packing fraction η and for $Q_1 = 0$ and $Q_1 = 2$. Fourteen system sizes in the range $20 \leq N \leq 2000$ have been used.
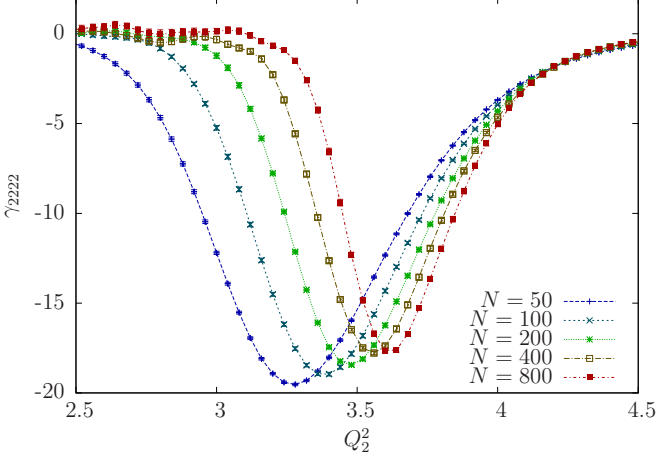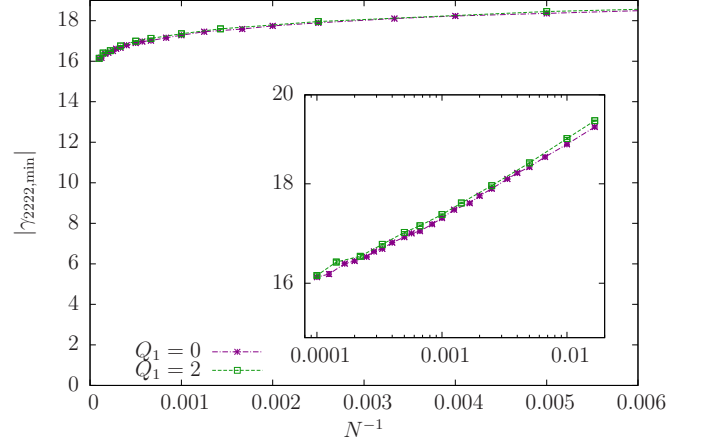

Figure 8: (Color online) The size of the dip in the fourth-order modulus $|\gamma_{2222,\min}|$ as a function of inverse system size N^{-1}. The packing fraction is $\eta = 5 \cdot 10^{-4}$, and results for $Q_1 = 0$ and $Q_1 = 2$ are shown. The inset shows the results on a log-log scale. System sizes in the range $60 \leq N \leq 10000$ are used.

Figure 7: (Color online) The fourth-order modulus γ_{2222} as a function of coupling Q_2^2 for five different system sizes N, when $Q_1 = 2$ and $\eta = 5 \cdot 10^{-4}$.
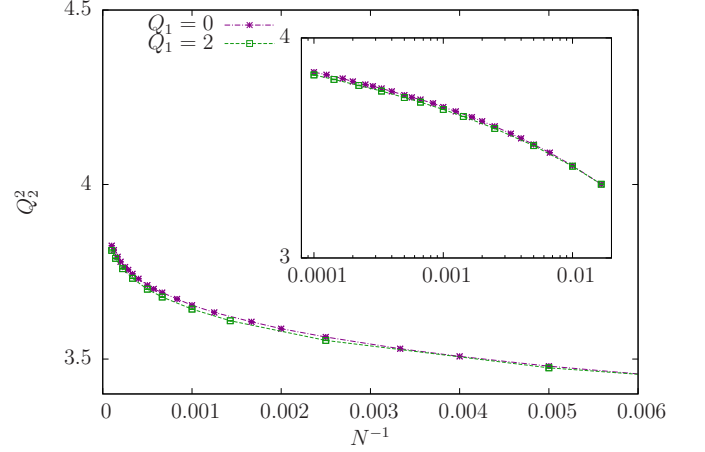

Figure 9: (Color online) The coupling value at the minimum of the dip in the fourth-order modulus as a function of inverse system size N^{-1}. The packing fraction is $\eta = 5 \cdot 10^{-4}$, and results for $Q_1 = 0$ and $Q_1 = 2$ are shown. The inset shows the results on a log-log scale. System sizes in the size $60 \leq N \leq 10000$ are used.

N increases towards the thermodynamic limit. However, assuming power-law dependence of $|\gamma_{2222,\min}|$, the positive curvature in the log-log plot indicates a nonzero value of $|\gamma_{2222,\min}|$ when $N \to \infty$, verifying a discontinuous jump in ϵ_{22}^{-1}, as expected for a BKT-transition. Again, we find that the results for $Q_1 = 2$ are very similar to $Q_1 = 0$.

We also associate the coupling value of the minimum in the dip in γ_{2222} with the critical point and the results are shown in Fig. 9 in the case when $\eta = 5 \cdot 10^{-4}$. Clearly, the position of the dip moves towards higher values of Q_2^2 when the system size increases. However, the evolution towards $N^{-1} = 0$ is too slow to make a sharp determination of Q_2^2 in this limit as also noted before[65,66]. With this method, we are not able to verify that $Q_{2,c}^2 \approx 4.4$, as

was found above in Fig. 5 for this density.

By assuming a universal value of the discontinuous jump for a BKT-transition, we may determine the critical point of the BKT-transition using Eq. (33) with only one free parameter as described in Appendix C. The results are given in Fig. 10. The critical values of Q_2^2 are very similar to what was obtained in Fig. 5, but are determined with greater accuracy. For both cases, the critical point appears at higher Q_2^2 when density increases. However, $Q_{2,c}^2$ is systematically lower at $Q_1 = 2$ compared to $Q_1 = 0$.

For the range of small densities that we have investigated, the Monte-Carlo results for the unconventional
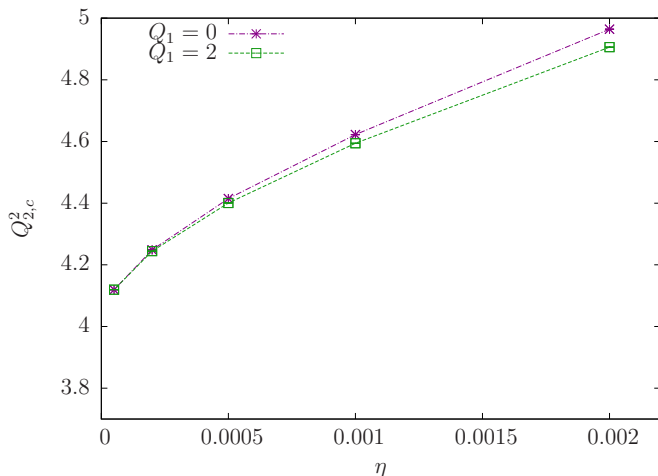
Figure 10: (Color online) The critical value of Q_2^2 found by curve-fitting to Eq. (33) with one free parameter. Results are presented for five values of the packing fraction η and for two values of Q_1.

Coulomb plasma with $Q_1 = 2$ are rather conclusive. This plasma undergoes a charge-unbinding transition that should be regarded as a BKT-transition in the sense that the inverse dielectric constant of type 2 exhibits the well-established signatures of a BKT-transition. Specifically, there is a density-dependent critical point $Q_{2,c}^2$ that separates a phase where particles of different species form bound pairs at high values of Q_2^2 from a phase where particles of different species are free at low values of Q_2^2. For test particles carrying type 2 charge, the high-Q_2^2 phase is unscreened, whereas the low-Q_2^2 phase is screened.

The results presented so far show that the behavior when $Q_1 = 0$ and $Q_1 = 2$ are quite similar. However, in the phase with bounded dipoles, when charges of type 2 are not screened, the cases $Q_1 = 0$ and $Q_1 = 2$ behave rather differently. We first consider the case when $Q_1 = 0$. When charges are bound, this system consists of N dipoles that interact by dipole-dipole interactions. Consequently, these dipoles tend to form clusters with increased dipole strength, i.e. higher values of the coupling or the density[15,29]. In Fig. 11, a snapshot of a $Q_1 = 0$ configuration with $N = 200$, $Q_2^2 = 7$ and $\eta = 2 \cdot 10^{-3}$ is shown, where some dipoles are seen to form clusters. In the case when $Q_1 = 2$, the type 2 interactions are effectively reduced to dipole-dipole interactions, similar to the $Q_1 = 0$ case. *However, the logarithmic interactions of type 1 charges remain.* Neglecting the weaker dipole-dipole interactions among dipoles of type two, the dipoles now essentially form elementary constituents with charge Q_1 interacting logarithmically. Effectively, the two-component unconventional plasma is reduced to a one-component plasma where the particles carry charge of type 1 and a (neutral) dipole of type 2. When $Q_1 = 2$ this plasma is in the liquid state, i.e. the tightly bound dipoles do not form an ordered state with a broken translational or orientational symmetry. Also, the logarithmic
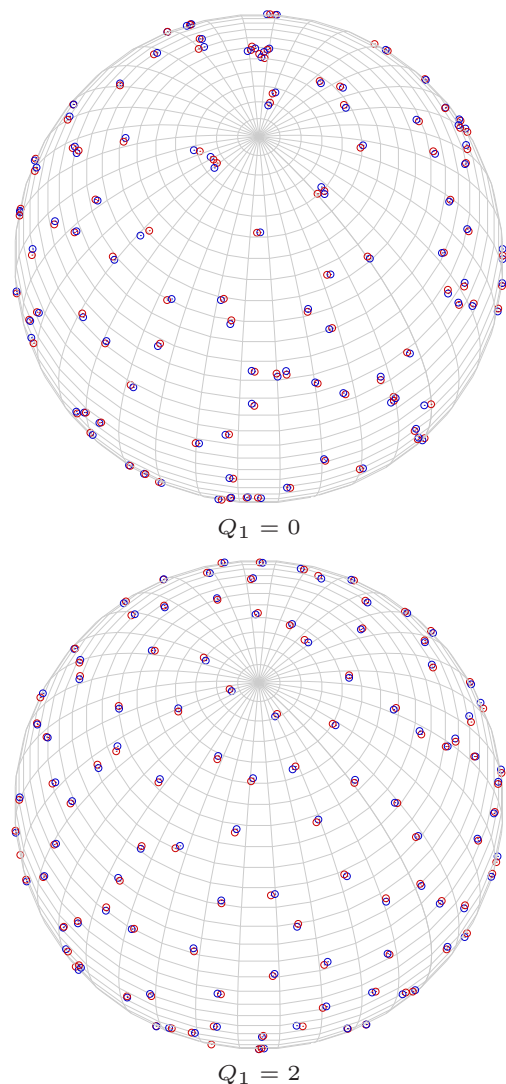

$Q_1 = 0$

$Q_1 = 2$

Figure 11: (Color online) Snapshots of the charge configuration at $Q_1 = 0$ and $Q_1 = 2$ when $Q_2^2 = 7$, $\eta = 2 \cdot 10^{-3}$, and $N = 200$. Red markers are w-particles and blue markers are z-particles. The marker diameters are about 2.5 times larger than hard disk diameter d.

interaction of type 1 charge will prevent the dipoles from forming clusters. A snapshot of the state with bounded dipoles when $Q_1 = 2$ is shown in Fig. 11 and the qualitative difference from the case when $Q_1 = 0$ is clearly seen. Quantitatively, this is seen by the behavior of ϵ_{22}^{-1}, presented in Fig. 12. When $Q_1 = 0$, dipole-dipole interactions at short distances will reduce the fluctuations in the dipole moment resulting in a weakly increasing ϵ_{22}^{-1} inside the bounded phase. On the other hand, when $Q_1 = 2$ the logarithmic interaction of type 1 charge will keep the dipoles at some distance from each other, thus the fluctuations of a dipole are not much restricted by the surrounding dipoles. Moreover, the strength of the dipoles increases with Q_2^2 and a reduction in ϵ_{22}^{-1} follows. The qualitative difference between the cases $Q_1 = 0$ and
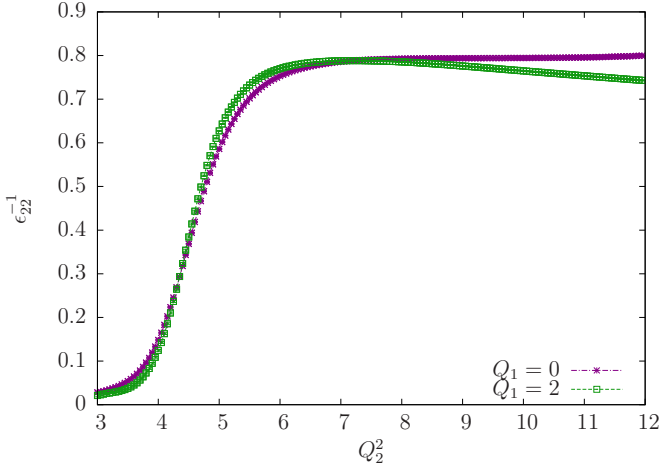
Figure 12: (Color online) Plot of the type 2 inverse dielectric constant for $Q_1 = 0$ and $Q_1 = 2$ with $N = 100$, $\eta = 5 \cdot 10^{-3}$ in the range $3 \leq Q_2^2 \leq 12$.

$Q_1 = 2$ is an effect due to the minimum separation of charges at finite density originating with the hard cores, and it will vanish in the limit $\eta \to 0$.

IV. CONCLUSIONS

We have shown that the unconventional Coulomb plasma analyzed in this paper, where particles can carry two distinct types of Coulombic charge, will screen test particles with charges of both types for the case most relevant for the plasma analogy of Ising-type fractional quantum Hall states, i.e. when there is one species of particles that carry type 1 charge $Q_1 = 2$ ($M = 2$) and type 2 charge $Q_2 = \sqrt{3}$ and another species of particles that carry only type 2 charge $-Q_2$. For test particles carrying both types of charge, screening will cease to occur at $Q_2^2 = Q_{2,c}^2 \approx 4$ in the limit of small density, when $Q_1 = 2$. For higher values of Q_2^2, the system will continue to screen test particles that carry only type 1 charge, but will not be able to screen test particles with type 2 charge.

One striking feature of these results is that $Q_{2,c}^2$ and the critical behavior at this point hardly seem to depend on Q_1 when density is small. This implies that the role of the type 1 interaction (which corresponds, in quantum Hall wavefunction language, to the Laughlin-Jastrow factor which accounts for the filling fraction of the system) is simply to maintain the z_i-particles in a liquid state. Since its critical point is very far away, the type 1 interaction leads to a weak, smooth dependence on Q_1. The physics in the transition at $Q_{2,c}^2$ is then dominated by the type 2 interaction. We therefore conjecture that our results hold for all reasonable values of M – not only $M = 0$ and 2, the cases which we have studied here, but also $M = 1$ (which may be relevant to ultra-cold trapped bosons) and larger values of M, possibly all the way up to or near the critical value $M_c \approx 70$, below which the one-component

plasma of Eq. (3) is in the metallic phase[33–36].

Appendix A: Generalizing the inverse dielectric constant for multiple interactions

In the unconventional plasma with two components that interact with two different Coulomb-like interactions, we are free to insert test particles that may interact with different charge strength through both interactions simultaneously. Here, we will generalize the inverse dielectric constant for such test particles. For consistency, we will also perform the derivation on the surface of a sphere by expanding in spherical harmonics. For a similar derivation, but with one interaction only and on a planar geometry, see Refs. 31,32.

When an external test charge field is inserted in the system, the free energy in the system will change according to the effective interaction among the test charges,

$$\Delta F[\delta q] = \int \mathrm{d}\Omega \int \mathrm{d}\Omega' \sum_{\mu,\nu} \delta q_\mu(\theta, \phi) U_{\mu\nu}^{\mathrm{eff}}(\hat{\mathbf{r}} \cdot \hat{\mathbf{r}}') \delta q_\nu(\theta', \phi').$$
(A1)

Here, the effective interaction between charges of type μ and ν, is assumed to be of the form $U_{\mu\nu}^{\mathrm{eff}} = U_{\mu\nu}^{\mathrm{eff}}(\hat{\mathbf{r}} \cdot \hat{\mathbf{r}}')$, $\delta q_\mu(\theta, \phi)$ is the test charge field for charges of type μ, and the integrations are over the solid angle $\mathrm{d}\Omega$. To correctly model the test particles as carrying charge of different types, we write

$$\delta q_\mu(\theta, \phi) = a_\mu \, \delta q \, \rho(\theta, \phi), \quad (A2)$$

where a_μ is a type dependent factor that accounts for the relative strength of charges of different types. For instance, the choice $(a_1, a_2) = (Q_1/MQ_2, 1) = (\sqrt{2/3M}, 1)$ describes the test charges corresponding to quasiholes in the MR state, as given in Eq. (125) in Ref. 2, which map

to particles in the plasma that carry charge $Q_1/2M = 1/\sqrt{2M}$ of type 1 and charge $Q_2/2 = \sqrt{3}/2$ of type 2. Moreover, in Eq. (A2) δq is a common charge factor for all types such that $a_\mu \delta q$ is the total charge of type μ carried by a test particle (which means that $\delta q = \sqrt{3}/2$ in the example above), and $\rho(\theta, \phi)$ is the density field of the test particles.

It is now convenient to expand the interaction and density fields in spherical harmonics. The test particle density field is expanded by

$$\rho(\theta, \phi) = \sum_{l=0}^{\infty} \sum_{m=-l}^{l} \rho_l^m Y_l^m(\theta, \phi), \qquad (A3)$$

where

$$Y_l^m(\theta, \phi) = \sqrt{\frac{(2l+1)(l-m)!}{4\pi(l+m)!}} P_l^m(\cos\theta)\, e^{im\phi}, \quad (A4)$$

and $P_l^m(x)$ are the associated Legendre polynomials. The coefficients are given by

$$\rho_l^m = \int d\Omega\, \rho(\theta, \phi) Y_l^{m*}(\theta, \phi). \qquad (A5)$$

The effective interaction is expanded by using the addition theorem for spherical harmonics,

$$U_{\mu\nu}^{\text{eff}}(\hat{\mathbf{r}} \cdot \hat{\mathbf{r}}') = \sum_{l=0}^{\infty} \frac{4\pi}{2l+1} U_{\mu\nu,l}^{\text{eff}} \sum_{m=-l}^{l} Y_l^{m*}(\theta, \phi) Y_l^m(\theta', \phi'). \qquad (A6)$$

Here, $U_{\mu\nu,l}^{\text{eff}}$ are the Legendre coefficients of the interaction, given by

$$U_{\mu\nu,l}^{\text{eff}} = \frac{2l+1}{2} \int_0^\pi d\theta\, \sin\theta\, U_{\mu\nu}^{\text{eff}}(\cos\theta) P_l(\cos\theta), \quad (A7)$$

where $P_l(x)$ is the Legendre polynomial of order l. Now Eq. (A1) is written

$$\Delta F[\delta q] = \delta q^2 \sum_{l=0}^{\infty} \frac{4\pi}{2l+1} \sum_{\mu,\nu} a_\mu U_{\mu\nu,l}^{\text{eff}} a_\nu \sum_{m=-l}^{l} \rho_l^{m*} \rho_l^m. \qquad (A8)$$

Hence, in the limit when the test charge field is infinitesimal, $\delta q \to 0$, we find that

$$\left. \frac{\partial^2 F[\delta q]}{\partial \delta q^2} \right|_{\delta q=0} = \sum_{l=0}^{\infty} \frac{8\pi}{2l+1} \sum_{\mu,\nu} a_\mu U_{\mu\nu,l}^{\text{eff}} a_\nu \sum_{m=-l}^{l} \rho_l^{m*} \rho_l^m. \qquad (A9)$$

This derivative can also be calculated by inspection of the partition function of the system perturbed with the external test charge field. With $F[\delta q] = -\ln Z[\delta q]$ and a potential energy on the form $V[\delta q] = V_0 + V_1[\delta q]$ where V_0 is the potential energy of the unperturbed system and $V_1[\delta q]$ is the contribution due to the test charge field, we

find that

$$\left. \frac{\partial^2 F[\delta q]}{\partial \delta q^2} \right|_{\delta q=0} = \left\langle \left. \frac{\partial^2 V_1[\delta q]}{\partial \delta q^2} \right|_{\delta q=0} \right\rangle$$
$$- \left\langle \left(\left. \frac{\partial V_1[\delta q]}{\partial \delta q} \right|_{\delta q=0} \right)^2 \right\rangle. \qquad (A10)$$

Here, we have also used that $\partial F[\delta q]/\partial \delta q|_{\delta q=0} = 0$, and the brackets denote statistical average with respect to the unperturbed system. The test charges $\delta q_\mu(\theta, \phi)$ will interact with each other as well as with the charge field $q_\mu(\theta, \phi)$. As for the test charge field, the charge field is expanded according to Eq. (A3) to yield

$$V_1[\delta q] = \int d\Omega \int d\Omega' \sum_\mu [q_\mu(\theta, \phi) + \delta q_\mu(\theta, \phi)]$$
$$\times U(\hat{\mathbf{r}} \cdot \hat{\mathbf{r}}') \delta q_\mu(\theta', \phi')$$
$$= \sum_{l=0}^{\infty} \frac{4\pi}{2l+1} U_l \sum_\mu a_\mu \sum_{m=-l}^{l} \delta q\, \rho_l^{m*} \left(q_{\mu,l}^m + a_\mu \delta q\, \rho_l^m \right), \qquad (A11)$$

where $U(\hat{\mathbf{r}} \cdot \hat{\mathbf{r}}')$ is the bare interaction, expanded by Eq. (A6) with coefficients U_l. Performing the derivatives in Eq. (A10) yields

$$\left. \frac{\partial^2 F[\delta q]}{\partial \delta q^2} \right|_{\delta q=0} = \sum_{l=0}^{\infty} \frac{8\pi}{2l+1} U_l \sum_{\mu,nu} a_\mu \delta_{\mu\nu} a_\nu \sum_{m=-l}^{l} \rho_l^{m*} \rho_l^m$$
$$- \sum_{l=0}^{\infty} \frac{4\pi}{2l+1} U_l \sum_{l'=0}^{\infty} \frac{4\pi}{2l'+1} U_{l'} \sum_{\mu,\nu} a_\mu a_\nu$$
$$\times \sum_{m=-l}^{l} \sum_{m'=-l'}^{l'} \rho_l^{m*} \rho_{l'}^{m'} \left\langle q_{\mu,l}^m q_{\nu,l'}^{m'*} \right\rangle. \qquad (A12)$$

We introduce the dielectric function $\epsilon_{\mu\nu,l}$ by

$$U_{\mu\nu,l}^{\text{eff}} = \epsilon_{\mu\nu,l}^{-1} U_l, \qquad (A13)$$

and by comparing Eqs. (A9) and (A12), the inverse dielectric function is found to be

$$\epsilon_{\mu\nu,l}^{-1} = \delta_{\mu\nu} - \left(\sum_{m=-l}^{l} \rho_l^{m*} \rho_l^m \right)^{-1} \sum_{l'=0}^{\infty} \frac{2\pi}{2l'+1} U_{l'}$$
$$\times \sum_{m=-l}^{l} \sum_{m'=-l'}^{l'} \rho_l^{m*} \rho_{l'}^{m'} \left\langle q_{\mu,l}^m q_{\nu,l'}^{m'*} \right\rangle. \quad (A14)$$

Moreover, since the bare interaction is only dependent on the distance between the charges, $U = U(\hat{\mathbf{r}} \cdot \hat{\mathbf{r}}')$, we

have that $\langle q_{\mu,l}^m q_{\nu,l'}^{m'*} \rangle = \langle q_{\mu,l}^m q_{\nu,l'}^{m'*} \rangle \delta_{ll'} \delta_{mm'}$, which yields

$$\epsilon_{\mu\nu,l}^{-1} = \delta_{\mu\nu} - \left(\sum_{m=-l}^{l} \rho_l^{m*} \rho_l^m \right)^{-1} \frac{2\pi}{2l+1} U_l$$
$$\times \sum_{m=-l}^{l} \rho_l^{m*} \rho_l^m \langle q_{\mu,l}^m q_{\nu,l}^{m*} \rangle. \quad (A15)$$

Additionally, the property that the bare interaction is distance dependent, only, yields an interaction U_l that is independent of m. Hence, the correlator $\langle q_{\mu,l}^m q_{\nu,l}^{m*} \rangle$ must be m independent as well, $\langle q_{\mu,l}^m q_{\nu,l}^{m*} \rangle = \langle q_{\mu,l}^0 q_{\nu,l}^0 \rangle$. The dielectric function thus reads

$$\epsilon_{\mu\nu,l}^{-1} = \delta_{\mu\nu} - \frac{2\pi}{2l+1} U_l \langle q_{\mu,l}^0 q_{\nu,l}^0 \rangle. \quad (A16)$$

The dielectric constant $\epsilon_{\mu\nu}$ is now found in the long wavelength limit of the dielectric function. On a spherical surface, this corresponds to setting $l=1$ in the dielectric function, i.e. $\epsilon_{\mu\nu} = \epsilon_{\mu\nu,1}$. Thus, the dielectric constant is

$$\epsilon_{\mu\nu}^{-1} = \delta_{\mu\nu} - \frac{2\pi}{3} U_1 \langle q_{\mu,1}^0 q_{\nu,1}^0 \rangle. \quad (A17)$$

So far, only a few assumptions are made regarding the bare interaction $U(\hat{\mathbf{r}} \cdot \hat{\mathbf{r}}')$ and the charge field $q_\mu(\theta, \phi)$. To apply Eq. (A17) for the system under consideration in this paper, we invoke $U(\hat{\mathbf{r}} \cdot \hat{\mathbf{r}}') = -\ln(1 - \hat{\mathbf{r}} \cdot \hat{\mathbf{r}}')$ to find $U_1 = 3/2$ by Eq. (A7). Moreover, the charge field is modeled as point charges in a uniform background

$$q_\mu(\theta, \phi) = q_\mu^{\mathrm{BG}} + \sum_{i=1}^{N} e_{\mu,i} \frac{\delta(\theta - \theta_i) \delta(\phi - \phi_i)}{\sin\theta}, \quad (A18)$$

where $q_\mu^{\mathrm{BG}} = -(\sum_i e_{\mu,i})/(4\pi)$ is the uniform background ensuring charge neutrality for charges of type μ, $e_{\mu,i}$ is the charge of type μ in particle i and the sum is over all N particles of the unperturbed system. Now, using Eq. (A5), the actual coefficient of the charge field is found to be

$$q_{\mu,1}^0 = \sqrt{\frac{3}{4\pi}} \frac{M_{\mu,z}}{R}, \quad (A19)$$

where $\mathbf{M}_\mu = \sum_{i=1}^{N} e_{\mu,i} \hat{\mathbf{r}}_i$ is the total dipole moment for charges of type μ. Finally, by inserting these results in Eq. (A17), the inverse dielectric constant is found to be

$$\epsilon_{\mu\nu}^{-1} = \delta_{\mu\nu} - \frac{\pi}{A} \langle \mathbf{M}_\mu \cdot \mathbf{M}_\nu \rangle, \quad (A20)$$

where $\langle M_{\mu,z} M_{\nu,z} \rangle = \langle \mathbf{M}_\mu \cdot \mathbf{M}_\nu \rangle / 3$ by assuming isotropy.

When there are test charges with multiple interactions, there are multiple contributions to the change in free energy as seen in Eq. (A1). To account for all contributions to the increase in free energy, we construct a generalized dielectric constant by

$$\epsilon_{(a_1, a_2, \dots)}^{-1} = \sum_{\mu, \nu} a_\mu \epsilon_{\mu\nu}^{-1} a_\nu. \quad (A21)$$

Notice that even though there is no bare interaction between charges of different type, there may be nonzero cross terms in Eq. (A1), as charges of different type are constrained to be together within the same particle.

Appendix B: Fourth-order free energy derivative

In Ref. 65 a method of verifying the discontinuous character of the BKT-transition was introduced, by examining a higher-order term in the free energy expansion in the XY-model when the system is perturbed with an infinitesimal phase twist. Similarly, in Ref. 66, the method was applied in a two-dimensional logarithmic plasma. Here, we show that the same idea also applies when we perturb a logarithmic Coulomb plasma on a spherical surface with an infinitesimal test charge field with multiple types of Coulomb interactions.

Consider a system with particles interacting with different charges of multiple types, as previously described. We now *choose* to perturb this system with a neutral distribution of test charge of multiple types, which has the form $\delta q_\mu(\theta) = a_\mu \delta q \cos(\theta)$, i.e. a similar test particle density field as given in Eq. (A2) but with $\rho_1^0 = \sqrt{4\pi/3}$ being the only nonzero coefficient in the spherical harmonics expansion. This is a convenient choice because it corresponds to the most long-waved nonuniform test charge configuration on the surface of a sphere, and hence, the prefactor of the second-order term in the free energy expansion will be the inverse dielectric constant, as we will see below.

The test charges yield a contribution to the potential energy as given by the $l=1$ and $m=0$ term in Eq. (A11),

$$V_1[\delta q] = \frac{4\pi}{3} U_1 \sum_\mu a_\mu \delta q \, \rho_1^0 \left(q_{\mu,1}^0 + a_\mu \delta q \rho_1^0 \right). \quad (B1)$$

We now consider how the system responds to the test charges by a Taylor expansion of the free energy in the test charge field around $\delta q = 0$,

$$\Delta F[\delta q] = \frac{\partial F[\delta q]}{\partial \delta q} \bigg|_{\delta q=0} \delta q + \frac{\partial^2 F[\delta q]}{\partial \delta q^2} \bigg|_{\delta q=0} \frac{\delta q^2}{2!}$$
$$+ \frac{\partial^3 F[\delta q]}{\partial \delta q^3} \bigg|_{\delta q=0} \frac{\delta q^3}{3!} + \frac{\partial^4 F[\delta q]}{\partial \delta q^4} \bigg|_{\delta q=0} \frac{\delta q^4}{4!} + \dots. \quad (B2)$$

The change in the free energy $\Delta F[\delta q]$ must be invariant to $\delta q_\mu(\theta) \to -\delta q_\mu(\theta)$, and hence, all odd-order derivatives in Eq. (B2) are zero. From Appendix A (see Eqs. (A12), (A17) and (A21)), the second-order free energy derivative is found to be

$$\frac{\partial^2 F[\delta q]}{\partial \delta q^2} \bigg|_{\delta q=0} = \frac{8\pi}{3} (\rho_1^0)^2 U_1 \epsilon_{(a_1, a_2, \dots)}^{-1}. \quad (B3)$$

The fourth-order derivative is

$$
\begin{aligned}
\frac{\partial^4 F[\delta q]}{\partial \delta q^4}\bigg|_{\delta q=0} &= 3\left\langle\left(\frac{\partial V_1[\delta q]}{\partial \delta q}\bigg|_{\delta q=0}\right)^2\right\rangle^2 \\
&\quad - \left\langle\left(\frac{\partial V_1[\delta q]}{\partial \delta q}\bigg|_{\delta q=0}\right)^4\right\rangle \\
&= \left(\frac{4\pi}{3}\rho_1^0 U_1\right)^4 \sum_{\mu,\nu,\rho,\sigma} a_\mu a_\nu a_\rho a_\sigma \\
&\quad \times\left[3\langle q_{\mu,1}^0 q_{\nu,1}^0\rangle\langle q_{\rho,1}^0 q_{\sigma,1}^0\rangle - \langle q_{\mu,1}^0 q_{\nu,1}^0 q_{\rho,1}^0 q_{\sigma,1}^0\rangle\right]. \quad \text{(B4)}
\end{aligned}
$$

where brackets denote a statistical average with respect to the unperturbed action. Inserting Eqs. (B3) and (B4) in Eq. (B2) yields

$$
\Delta F[\delta q] = \frac{8\pi}{3}(\rho_1^0)^2 U_1\left[\epsilon_{(a_1,a_2,\dots)}^{-1}\frac{\delta q^2}{2!} + \gamma_{(a_1,a_2,\dots)}\frac{\delta q^4}{4!} + \dots\right], \quad \text{(B5)}
$$

where

$$
\gamma_{(a_1,a_2,\dots)} = \sum_{\mu,\nu,\rho,\sigma} a_\mu a_\nu a_\rho a_\sigma \gamma_{\mu\nu\rho\sigma}, \quad \text{(B6)}
$$

and

$$
\begin{aligned}
\gamma_{\mu\nu\rho\sigma} = \left(\frac{4\pi}{3}U_1\right)^3 \frac{(\rho_1^0)^2}{2}\big[&3\langle q_{\mu,1}^0 q_{\nu,1}^0\rangle\langle q_{\rho,1}^0 q_{\sigma,1}^0\rangle \\
&- \langle q_{\mu,1}^0 q_{\nu,1}^0 q_{\rho,1}^0 q_{\sigma,1}^0\rangle\big]. \quad \text{(B7)}
\end{aligned}
$$

Now, inserting $\rho_1^0 = \sqrt{4\pi/3}$ and assuming the charge field in Eq. (A18) and a logarithmic bare interaction, $U_1 = 3/2$, yields

$$
\begin{aligned}
\gamma_{\mu\nu\rho\sigma} = \left(\frac{\pi}{R^2}\right)^2\big[&\langle\mathbf{M}_\mu\mathbf{M}_\nu\rangle\langle\mathbf{M}_\rho\mathbf{M}_\sigma\rangle \\
&- 3\langle M_{\mu,z}M_{\nu,z}M_{\rho,z}M_{\sigma,z}\rangle\big], \quad \text{(B8)}
\end{aligned}
$$

where $\langle M_{\mu,z}M_{\nu,z}\rangle = \langle\mathbf{M}_\mu\cdot\mathbf{M}_\nu\rangle/3$ by assuming isotropy.

1. Stability argument

When $\delta q = 0$, the free energy of the system has a global minimum, and hence, the right-hand side of Eq. (B5) must be greater or equal to zero. Now, if $\gamma_{(a_1,a_2,\dots)}$ approaches a nonzero negative value at the critical point in the thermodynamical limit, the general inverse dielectric constant must simultaneously have a nonzero positive value for the ground state to be stable. However, since $\epsilon_{(a_1,a_2,\dots)}^{-1} = 0$ in the screening phase, it follows that $\epsilon_{(a_1,a_2,\dots)}^{-1}$ must exhibit a discontinuous jump at the critical point. Hence, investigation of $\gamma_{(a_1,a_2,\dots)}$ may be used to verify a discontinuity in the inverse dielectric constant, which is a necessary requirement for observing a BKT-transition.

Appendix C: The finite-size scaling relation

The finite-size scaling relation of the BKT-transition has been used throughout this article to verify the universal jump in ϵ_{22}^{-1} and to provide estimates for the critical coupling $Q_{2,\text{c}}^2$. Here, some details to the curve fitting procedure and the goodness of fit measure are presented.

1. Two free parameters

Least-squares curve fitting of the Monte-Carlo results for ϵ_{22}^{-1} to Eq. (33) may be performed with both $\epsilon_{22}^{-1}(\infty)$ and C as free parameters[28,30,72,73]. If the transition is of the BKT-type, a good fit to Eq. (33) should be obtained at the critical point. In addition, when $\epsilon_{22}^{-1}(\infty)$ is free, no *a priori* assumption on the value of the universal jump is made, thus a resulting value of $\epsilon_{22}^{-1}(\infty)$ that corresponds to the universal jump of the BKT-transition should be obtained. However, with two free parameters, higher quality of the Monte-Carlo statistics is required to single out when they system is closely obeying the behavior of Eq. (33).

We have employed the Marquardt-Levenberg algorithm minimizing χ^2 to the nonlinear fitting function in Eq. (33). Specifically, χ^2 is the sum of squared weighted residuals,

$$
\chi^2 = \sum_{i=1}^n \left(\frac{\epsilon_{22,N_i}^{-1} - \epsilon_{22}^{-1}(N_i)}{\sigma_{N_i}}\right)^2, \quad \text{(C1)}
$$

where n is the number of system sizes N_i, ϵ_{22,N_i}^{-1} is the value of the inverse dielectric constant ϵ_{22}^{-1} obtained from the Monte-Carlo simulation at system size N_i, and σ_{N_i} is the corresponding error. For a good fit, we expect the weight-normalized residuals, $Y_i = (\epsilon_{22,N_i}^{-1} - \epsilon_{22}^{-1}(N_i))/\sigma_{N_i}$ to be Gaussian-distributed with mean $\mu(Y_i) = 0$ and variance $\sigma^2(Y_i) = 1$. Thus, to measure the goodness of the fit, we use the Anderson-Darling test statistic A^2 for the data set Y_i to arise from a normal distribution with $\mu(Y_i) = 0$ and $\sigma^2(Y_i) = 1$:

$$
A^2 = -n - \frac{1}{n}\sum_{i=1}^n (2i-1)\{\ln[\Phi(Y_i)] + \ln[\Phi(Y_{n+1-i})]\},
$$
$$\text{(C2)}$$

where $\Phi(Y)$ is the standard normal cumulative distribution function and where the data set Y_i is ordered from low to high values. A smaller value of A^2 essentially means a better fit between the data and the fit function.

To illustrate the method, Monte-Carlo results for ϵ_{22}^{-1} at fourteen different system sizes and the corresponding curve-fit according to Eq. (33) are given in Fig. 13 for three different values of Q_2^2. Here, $\eta = 2\cdot 10^{-3}$ and $Q_1 = 0$. Clearly, at $Q_2^2 = 4.933$, the fit between the data and the fit function is better than for the two other cases. Moreover, in Fig. 14 the corresponding results for the goodness of fit parameter as well as the results for
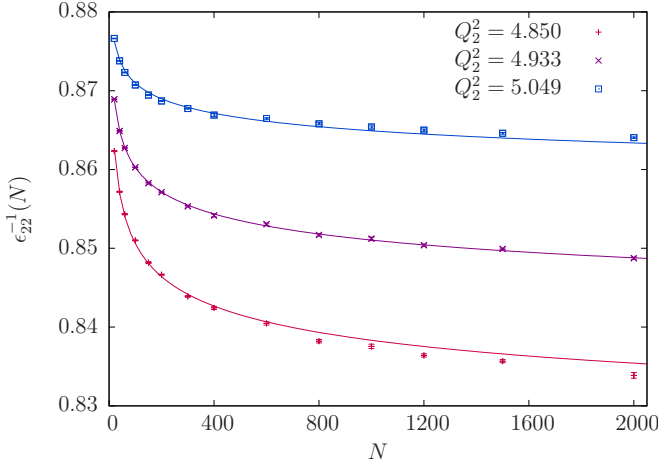
Figure 13: (Color online) Plot of the size-dependence in the inverse dielectric constant $\epsilon_{22}^{-1}(N)$ for fourteen different system sizes in the range $20 \leq N \leq 2000$ at three different values of the coupling Q_2^2. The best fit according to the fit function in Eq. (33) with two free parameters, is given as the corresponding solid line in all three cases. The packing fraction is $\eta = 2 \cdot 10^{-3}$ and $Q_1 = 0$.

the parameter $\epsilon_{22}^{-1}(\infty)$ as a function of Q_2^2 are shown. Indeed, the minimum in A^2 indicates a critical region where the data seem to follow the logarithmic finite size scaling of ϵ_{22}^{-1} given in Eq. (33). Also note that this region coincides with a value of $Q_2^2 \epsilon_{22}^{-1}(\infty)$ close to the universal jump value of 4. With the minimum of A^2 as a measure of the critical point and with error estimates obtained by the Jackknife method, we find that $Q_{2,c}^2 = 4.933 \pm 0.012$ and that $Q_{2,c}^2 \epsilon_{22}^{-1}(\infty) = 3.941 \pm 0.023$, less than 2% off the universal number. The results in Figs. 5 and 6 are found by repeating this procedure for different values of η and Q_1.

2. One free parameter

The procedure described in detail above with two free parameters, may be performed with a fixed value of $\epsilon_{22}^{-1}(\infty) = 4Q_{2,c}^2$ and with C as the only free parameter. If the transition is of the BKT-type, a good fit to Eq. (33) should be obtained at the critical point. This is a rather well-used method to determine the critical point of a BKT-transition[29,72,74,75]. With only one free parameter, $Q_{2,c}^2$ will be determined with greater accuracy

compared to the case when there are two free parameters.

3. Remarks

Refs. 28 and 30 used χ^2 as a goodness of fit parameter. We also tried this, and the results for the critical coupling as well as the corresponding parameter $\epsilon_{22}^{-1}(\infty)$ were consistent with A^2 results within statistical uncertainty.
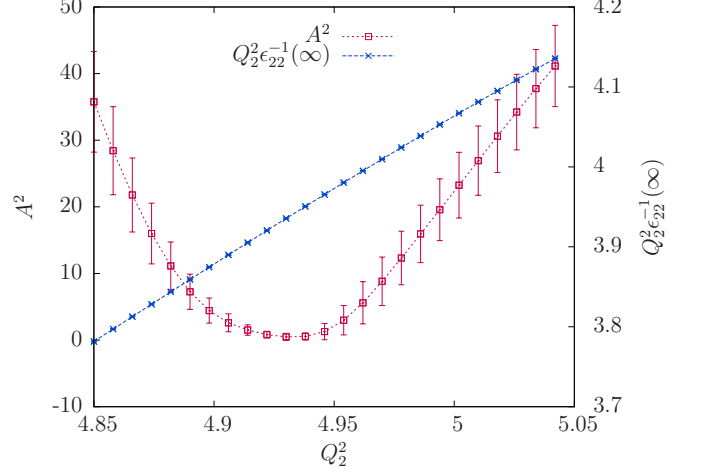

Figure 14: (Color online) Plot of the goodness of fit parameter A^2 and the corresponding free parameter $\epsilon_2^{-1}(\infty)$ obtained when curve fitting to the critical finite-size relation given in Eq. (33). The results are given as a function of Q_2^2. System sizes N, and η and Q_1 are the same as in Fig. 13. Error estimates are obtained by the Jackknife method.

However, we found that error estimates were clearly underestimated with χ^2, probably due to over-fitting.

The parameter C in the finite-size scaling relation (Eq. (33)) is density dependent[76]. Specifically, C increases when η decreases. Hence, at the critical point, the finite-size scaling slows down when η is lowered. Therefore, larger systems N or better statistics are required to resolve the critical scaling when η is small. In particular, curve fitting to Eq. (33) was also performed for $\eta = 5 \cdot 10^{-5}$ in addition to the densities presented in Figs. 5 and 6. However, in this case the statistics were not good enough to resolve a clear minimum in A^2. Also note that there are higher-order corrections[76] to Eq. (33) that are not taken into account in this work.

[1] R. B. Laughlin, Phys. Rev. Lett. **50**, 1395 (1983).

[2] P. Bonderson, V. Gurarie, and C. Nayak, Phys. Rev. B **83**, 075303 (2011).

[3] G. Moore and N. Read, Nucl. Phys. B **360**, 362 (1991).

[4] S.-S. Lee, S. Ryu, C. Nayak, and M. P. A. Fisher, Phys. Rev. Lett. **99**, 236807 (2007), arXiv:0707.0478.

[5] M. Levin, B. I. Halperin, and B. Rosenow, Phys. Rev. Lett. **99**, 236806 (2007), arXiv:0707.0483.

[6] P. Bonderson and J. K. Slingerland, Phys. Rev. B **78**, 125323 (2008), arXiv:0711.3204.

[7] R. Willett, J. P. Eisenstein, H. L. Stormer, D. C. Tsui, A. C. Gossard, and J. H. English, Phys. Rev. Lett. **59**,

1776 (1987).

[8] W. Pan, J.-S. Xia, V. Shvarts, D. E. Adams, H. L. Stormer, D. C. Tsui, L. N. Pfeiffer, K. W. Baldwin, and K. W. West, Phys. Rev. Lett. **83**, 3530 (1999), cond-mat/9907356.

[9] J. P. Eisenstein, K. B. Cooper, L. N. Pfeiffer, and K. W. West, Phys. Rev. Lett. **88**, 076801 (2002), cond-mat/0110477.

[10] J. S. Xia, W. Pan, C. L. Vicente, E. D. Adams, N. S. Sullivan, H. L. Stormer, D. C. Tsui, L. N. Pfeiffer, K. W. Baldwin, and K. W. West, Phys. Rev. Lett. **93**, 176809 (2004), cond-mat/0406724.

[11] N. Read and D. Green, Phys. Rev. B **61**, 10267 (2000), cond-mat/9906453.

[12] J. M. Kosterlitz and D. J. Thouless, J. Phys. C **6**, 1181 (1973).

[13] J. M. Kosterlitz, J. Phys. C **7**, 1046 (1974).

[14] J. M. Caillol and D. Levesque, Phys. Rev. B **33**, 499 (1986).

[15] G. Orkoulas and A. Z. Panagiotopoulos, J. Chem. Phys. **104**, 7205 (1996).

[16] E. K. Dahl, E. Babaev, and A. Sudbø, Phys. Rev. B **78**, 144510 (2008), arXiv:0807.0233.

[17] E. K. Dahl, E. Babaev, and A. Sudbø, Phys. Rev. Lett. **101**, 255301 (2008), arXiv:0810.3833.

[18] J. Smiseth, E. Smørgrav, E. Babaev, and A. Sudbø, Phys. Rev. B **71**, 214509 (2005), arXiv:cond-mat/0411761.

[19] E. V. Herland, E. Babaev, and A. Sudbø, Phys. Rev. B **82**, 134511 (2010), arXiv:1006.3311.

[20] E. Babaev, Phys. Rev. B **77**, 054512 (2008), arXiv:cond-mat/0611386.

[21] Without the hard-core repulsion, the system will be unstable at high coupling when one charge from each species together will form a pair with infinite negative energy.[22–24]

[22] R. M. May, Phys. Lett. A **25**, 282 (1967).

[23] G. Knorr, Phys. Lett. A **28**, 166 (1968).

[24] E. H. Hauge and P. C. Hemmer, Phys. Norv. **5**, 209 (1971).

[25] V. L. Berezinskii, Sov. Phys. JETP **32**, 493 (1971).

[26] P. Minnhagen, Rev. Mod. Phys **59**, 1001 (1987).

[27] Y. Saito and H. Müller-Krumbhaar, Phys. Rev. B **23**, 308 (1981).

[28] J.-R. Lee and S. Teitel, Phys. Rev. B **46**, 3247 (1992).

[29] J. Lidmar and M. Wallin, Phys. Rev. B **55**, 522 (1997), arXiv:cond-mat/9607025.

[30] P. Gupta and S. Teitel, Phys. Rev. B **55**, 2756 (1997), arXiv:cond-mat/9609031.

[31] P. Olsson, Phys. Rev. B **46**, 14598 (1992).

[32] P. Olsson, Phys. Rev. B **52**, 4511 (1995).

[33] S. W. de Leeuw and J. W. Perram, Physica A **113**, 546 (1982).

[34] J. M. Caillol, D. Levesque, J. J. Weis, and J. P. Hansen, J. Stat. Phys. **28**, 325 (1982).

[35] Ph. Choquard and J. Clerouin, Phys. Rev. Lett. **50**, 2086 (1983).

[36] M. Franz and S. Teitel, Phys. Rev. Lett. **73**, 480 (1994), arXiv:cond-mat/9403071.

[37] B. I. Halperin and D. R. Nelson, Phys. Rev. Lett. **41**, 121 (1978).

[38] D. R. Nelson and B. I. Halperin, Phys. Rev. B **19**, 2457 (1979).

[39] A. P. Young, Phys. Rev. B **19**, 1855 (1979).

[40] K. Chen, T. Kaplan, and M. Mostoller, Phys. Rev. Lett. **74**, 4019 (1995).

[41] J. Dietel and H. Kleinert, Phys. Rev. B **73**, 024113 (2006), arXiv:cond-mat/0508780.

[42] S. I. Lee and S. J. Lee, Phys. Rev. E **78**, 041504 (2008).

[43] A. Pérez-Garrido and M. A. Moore, Phys. Rev. B **58**, 9677 (1998), arXiv:cond-mat/9802167.

[44] J. O'Neill and M. A. Moore, Phys. Rev. B **48**, 374 (1993).

[45] M. J. W. Dodgson and M. A. Moore, Phys. Rev. B **55**, 3816 (1997), arXiv:cond-mat/9512123.

[46] M. A. Moore and A. Pérez-Garrido, Phys. Rev. Lett. **82**, 4078 (1999), arXiv:cond-mat/9812039.

[47] P. A. McClarty and M. A. Moore, Phys. Rev. B **75**, 172507 (2007), arXiv:cond-mat/0702282.

[48] V. S. Dotsenko and V. A. Fateev, Nucl. Phys. B **240**, 312 (1984).

[49] G. Felder, Nucl. Phys. B **317**, 215 (1989).

[50] S. D. Mathur, Nucl. Phys. B **369**, 433 (1992).

[51] R. E. Hetzel, A. Sudbø, and D. A. Huse, Phys. Rev. Lett. **69**, 518 (1992).

[52] S. Ryu and D. Stroud, Phys. Rev. B **57**, 14476 (1998), arXiv:cond-mat/9712246.

[53] P. Olsson and S. Teitel, Phys. Rev. B **67**, 144514 (2003), arXiv:cond-mat/0212471.

[54] S. Kragset, E. Babaev, and A. Sudbø, Phys. Rev. Lett. **97**, 170403 (2006), arXiv:cond-mat/0604416.

[55] E. Fradkin, B. A. Huberman and S. H. Shenker, Phys. Rev. B **18**, 4789 (1978).

[56] T. Chen and S. Teitel, Phys. Rev. B **55**, 15197 (1997), arXiv:cond-mat/9702010.

[57] A. F. Andreev and E. Bashkin, Sov. Phys. JETP **42**, 164 (1975).

[58] A. B. Kuklov and B. V. Svistunov Phys. Rev. Lett. **90**, 100401 (2003), arXiv:cond-mat/0205069.

[59] A. Kuklov , N. Prokof'ev, and B. Svistunov Phys. Rev. Lett. **92**, 050402 (2004), arXiv:cond-mat/0306662.

[60] J. W. Perram and S. W. de Leeuw, Physica A **109**, 237 (1981).

[61] L. Greengard and V. Rokhlin, J. Comput. Phys. **73**, 325 (1987).

[62] A. C. Maggs and V. Rossetto, Phys. Rev. Lett. **88**, 196402 (2002), arXiv:cond-mat/0111009.

[63] J. M. Caillol and D. Levesque, J. Chem. Phys. **94**, 597 (1991).

[64] A. Pérez-Garrido, M. J. W. Dodgson, and M. A. Moore, Phys. Rev. B **56**, 3640 (1997), arXiv:cond-mat/9701090.

[65] P. Minnhagen and B. J. Kim, Phys. Rev. B **67**, 172509 (2003), arXiv:cond-mat/0304226.

[66] K. Børkje, S. Kragset, and A. Sudbø, Phys. Rev. B **71**, 085112 (2005), arXiv:cond-mat/0412281.

[67] N. Metropolis, A. W. Rosenbluth, M. N. Rosenbluth, A. H. Teller, and E. Teller, J. Chem. Phys. **21**, 1087 (1953).

[68] W. K. Hastings, Biometrika **57**, 97 (1970).

[69] M. Matsumoto and T. Nishimura, ACM Trans. Model. Comput. Simul. **8**, 3 (1998).

[70] A. M. Ferrenberg and R. H. Swendsen, Phys. Rev. Lett. **61**, 2635 (1988).

[71] A. M. Ferrenberg and R. H. Swendsen, Phys. Rev. Lett. **63**, 1195 (1989).

[72] H. Weber and P. Minnhagen, Phys. Rev. B **37**, 5986 (1988).

[73] P. Minnhagen and H. Weber, Physica B **152**, 50 (1988).

[74] L. Bonnes and S. Wessel, Phys. Rev. Lett. **106**, 185302 (2011), arXiv:1101.5991.

[75] H. Kuroyanagi, M. Tsukamoto, and M. Tsubota, J. Low Temp. Phys. **162**, 609 (2011).

[76] P. Olsson and P. Minnhagen, Physica Scripta **43**, 203 (1991).